IOPscience iopscience.iop.org

Home Search Collections Journals About Contact us My IOPscience

A rigid dumbbell settling under gravity in a periodic flow field

This article has been downloaded from IOPscience. Please scroll down to see the full text article.

2009 J. Phys. A: Math. Theor. 42 025501

(http://iopscience.iop.org/1751-8121/42/2/025501)

View the table of contents for this issue, or go to the journal homepage for more

Download details:
IP Address: 171.66.16.154
The article was downloaded on 03/06/2010 at 07:46

Please note that terms and conditions apply.

IOP PUBLISHING JOURNAL OF PHYSICS A: MATHEMATICAL AND THEORETICAL

J. Phys. A: Math. Theor. **42** (2009) 025501 (19pp) doi:10.1088/1751-8113/42/2/025501

A rigid dumbbell settling under gravity in a periodic flow field

M F Piva and G R Martino

Grupo de Medios Porosos, Facultad de Ingeniería, Universidad de Buenos Aires, Paseo Colón 850 (1063), Buenos Aires Argentina

E-mail: mpiva@fi.uba.ar

Received 23 July 2008, in final form 27 October 2008
Published 25 November 2008
Online at stacks.iop.org/JPhysA/42/025501

Abstract

The motion of a rigid dumbbell settling under gravity in a stationary two-dimensional cellular flow field is investigated. The dumbbell is modeled as two identical beads connected by a rigid rod. Assuming that the bead radius is much shorter than the bead to bead distance, a simple model is obtained to describe the dynamical behavior of the dumbbell in terms of evolution of the dumbbell orientation and the velocity of the center of mass. The average velocity of the dumbbell in the gravity direction was found to depend on the dumbbell length, the inertia parameter and the terminal settling velocity in still fluid. For certain conditions the dumbbell remains suspended in the flow field. In one of the suspension regimes the dumbbell remains indefinitely attached to a fixed point. This behavior is related to the existence to saddle nodes in the cellular flow field.

PACS numbers: 92.10.Wa, 82.35.Lr, 05.60.−K

1. Introduction

In this paper we numerically investigate the advection of a dumbbell-shaped particle settling under gravity in a non-homogeneous periodic flow. In recent years, the transport properties of immersed particles have been the object of considerable research due to their numerous scientific and engineering applications. Examples are the motion of aerosols or contaminants in the atmosphere, suspension and sedimentation in rivers, migration of microorganisms in the ocean, motion of red blood cells in capillaries or fiber motion in flows of rheological interest.

A common hypothesis when considering the motion of such particles is that they are spherical in shape. This assumption allows the development of simple mathematical models [1] that successfully describe the particle dynamics in cases where it is more or less rounded or its shape is not far deviated from sphericity. In nature or in industrial applications, however,

 © 2009 IOP Publishing Ltd Printed in the UK

particles vary in a wide range of shapes, from near spherical or ellipsoidal to highly irregular shapes as compound aggregates.

The motion of non-spherical particles may be much more complex than those of spheres due to the coupling between the orientation and translational motions [2, 3]. In a moving fluid there is an additional source of complexity because of the interaction between the flow kinematics and the particle orientation [4, 5]. It is well known that induced-by-flow particle alignment plays an important role in determining the physical properties of a solution. As an example, the addition of fibers to a Newtonian fluid can change the flow kinematics due to flow-induced fiber alignment [6]. Moreover, the tendency of elongated particles to align their major axis along the shear rate could lead the system to exhibit anisotropy [7].

This flow-induced particle alignment may also be of importance in other scenarios where the shear flow effects are accompanied by the presence of an external force field. An important example occurs during the settling of heavy particles in a gravitational field. In still fluid, settling velocity of non-spherical particles will depend on the particle orientation with respect to gravity. However, in the cases were the fluid is in motion, the settling process could be affected by the interaction between the particle and the shear rate field. Mallier *et al* [8] studied the motion of ellipsoidal particles in a non-homogeneous two-dimensional flow field which has zero average velocity. He found that spherical particles without inertia fall on average with the still fluid settling velocity, while non-spherical particles settle on average more rapidly. He concluded that departures from the spherical shape have a negative incidence on particle suspension. However, he dedicated his study to ellipsoidal particles and did not consider any other possibilities.

The question that arises is if similar effects should be expected for distinct particle shapes than elliptic. Non-elliptic particles are common in several systems involving emulsions, dust, polymers, slurries or any other small particles that can get attached to form flocs or composite aggregates with lobes and large surface protuberances. In such cases, the ellipsoid might not be the most appropriate model for particle shape because it does not consider the effects of inhomogeneous mass distribution or the effects of shape irregularities on the forces exerted by the fluid. A simple case study which allows us to overcome the limitations of the ellipsoidal model is the rigid dumbbell. In general, a dumbbell shaped particle is a non-spherical structure with two lobes connected by a handle. In its simplest version it consists of two spheres separated by a fixed distance and connected by a rigid rod of negligible mass. This ideal model is on the basis of many studies on the hydrodynamics of arbitrary shaped particles [9] and particularly it has been extensively employed in the study of polymers [10]. Recently the authors considered the problem of an elastic dumbbell settling under gravity in a periodic flow and subjected to Brownian forces [11]. Their analysis of the interaction between the dumbbell and the flow field showed the existence of stability regions where the dumbbell can be eventually trapped for a long time. The existence of such basins of attraction proved to have a crucial role in the settling process affecting the values of mean quantities as the average settling velocity.

The purpose of this paper is to analyze the dynamical response of a falling dumbbell in a cellular flow field similar of those considered in Maxey works. We will determine the existence of regimes of permanent suspension with the emphasis put on the differences with the case of a single sphere in identical flow conditions. In order to capture the main features of the dumbbell dynamics we will restrict the analysis to the particular case of identical spheres which are more dense than the surrounding fluid. In this context, the motion of each particle can be described by a second-order integro-differential equation that has the particle inertia, viscous drag and gravity forces as the main components [12, 13]. Other forces such as the

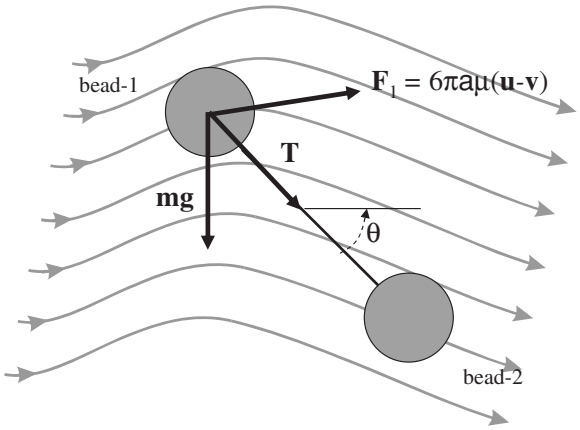

Figure 1. Schematic of the physical problem.

Basset history force, pressure gradient or added mass force, significant only when the particle density is of the order of the fluid density [1, 14], will be neglected.

A key point of the present analysis is that suspension occurs when dumbbells approach flow locations where the net force on the spheres is null. As will be shown, this phenomenon involves the combined effect of the bipolar particle geometry and the topological flow structure containing saddle points. Considering that the above conjecture does not imply any particular condition on the length of the dumbbell it will be taken large enough so the hydrodynamics interaction between the beads could be neglected.

The paper is organized as follows: the dimensionless motion equations of the dumbbell in a 2D cellular flow field are derived in section 2. In section 3 we present some examples of dumbbell trajectories showing the main features of the settling process. Section 4 is devoted to analyze the average settling velocity as a function of the dumbbell length. In section 5, dumbbell suspension is interpreted in terms of the existence of stable fixed points. Finally section 6 is devoted to conclusion and perspectives.

2. Equation for dumbbell motion

Consider a dumbbell shaped body settling under gravity in a stationary flow field $\mathbf{u}(\mathbf{r})$ as sketched in figure 1. Two identical beads, labeled 1 and 2, with mass m and radius R are connected by a thin rigid rod so that the distance between the mass centers of the beads is d. It is assumed that the mass and the hydrodynamic resistance of the rod are negligible compared to those of the beads and it will be considered that the beads are sufficient far apart for hydrodynamic interaction between them to be negligible. This last assumption implies that $d \gg R$. In addition, buoyancy forces on the bead will be ignored by assuming that the fluid density is negligible compared to that of the particles.

Provided that the beads are sufficiently small, the position $\mathbf{r}_i(t)$ of each bead and their velocity $\mathbf{v}_i(t)$ are in first approximation

$$m\ddot{\mathbf{r}}_1 = \mathbf{F}_1 + \mathbf{T} + m\mathbf{g} \tag{1}$$

$$m\ddot{\mathbf{r}}_2 = \mathbf{F}_2 - \mathbf{T} + m\mathbf{g} \tag{2}$$

where $\mathbf{F_i}$, the hydrodynamic force on the bead i, is, by Stokes' law

$$\mathbf{F_i} = \beta[\mathbf{u}(\mathbf{r_i}) - \mathbf{v_i}] \tag{3}$$

with $\beta = 6\pi\mu R$ being the Stokes drag coefficient for a bead and $\mathbf{T}$ a constraint force acting on each bead and directed along the beads line of center.

As an alternative, the motion of the dumbbell can be completely specified by the instantaneous velocity $\mathbf{V} = (\mathbf{V_1} + \mathbf{V_2})/2$ of its mass center, $\mathbf{r} = (\mathbf{r_1} + \mathbf{r_2})/2$ and the instantaneous angular velocity Ω about this point.

An equation for the translational motion of the dumbbell mass center can be obtained by adding equations (1) and (2) to give

$$m\frac{\mathrm{d}\mathbf{V}}{\mathrm{d}t} = \beta\left[\frac{1}{2}(\mathbf{u_2} + \mathbf{u_1}) - \mathbf{V} + \mathbf{W}\right], \tag{4}$$

where $\mathbf{W} = m\mathbf{g}/\beta$ is the terminal fall velocity for a bead in still fluid.

The rotational dynamics of the dumbbell can be obtained from the angular momentum equation for a rigid body. Denoting $\mathbf{L}$, the angular momentum measured about the mass center of the dumbbell and $\mathbf{M}$ the external torques acting on each bead, the evolution of $\mathbf{L}$ is described by

$$\frac{\mathrm{d}\mathbf{L}}{\mathrm{d}t} = \mathbf{M_1} + \mathbf{M_2}, \tag{5}$$

where $\mathbf{M_1} = \mathbf{d/2} \times \mathbf{F_1}$, $\mathbf{M_2} = -\mathbf{d/2} \times \mathbf{F_2}$ and $\mathbf{d} = \mathbf{r_2} - \mathbf{r_1}$ the connector vector between beads.

If the dumbbell is constrained to move in the $x - y$ plane the direction of the angular velocity vector is along the z-axis and the angular momentum is given by $\mathbf{L} = I\Omega$. Substituting into equation (5) it is obtained

$$I\frac{\mathrm{d}\Omega}{\mathrm{d}t} = \frac{\beta}{2}[\mathbf{d} \times (\mathbf{u_2} - \mathbf{u_1}) - d^2\Omega\hat{z}], \tag{6}$$

where

$$I = \frac{4}{5}mR^2 + m\frac{d^2}{2} \tag{7}$$

is the moment of inertia about the principal axis of the dumbbell. As an example we consider the motion of the dumbbell in still fluid. In this case $\mathbf{u_1} = \mathbf{u_2} = 0$ and thus equations (4) and (6) become:

$$m\frac{\mathrm{d}\mathbf{V}}{\mathrm{d}t} = \beta[-\mathbf{V} + \mathbf{W}] \tag{8}$$

$$I\frac{\mathrm{d}\Omega}{\mathrm{d}t} = -\frac{d^2\beta}{2}\Omega\hat{z}. \tag{9}$$

For arbitrary values of $\mathbf{V_o}$, the initial center-of-mass velocity and $\Omega_\mathbf{o}$, the initial angular velocity of the dumbbell principal axis, the solutions are

$$\mathbf{V} = (\mathbf{V_o} - \mathbf{W})e^{-}t/\tau_1 + \mathbf{W} \tag{10}$$

$$\Omega = \Omega_\mathbf{o}e^{-}t/\tau_2 \tag{11}$$

with $\tau_1 = \beta/m$ and $\tau_2 = \beta/(2Id^2)$. If for example $\mathbf{V_o} = 0$ and $\Omega_\mathbf{o} = 0$ then the dumbbell settles out without rotation and with terminal velocity $\mathbf{V} = \mathbf{W}$.

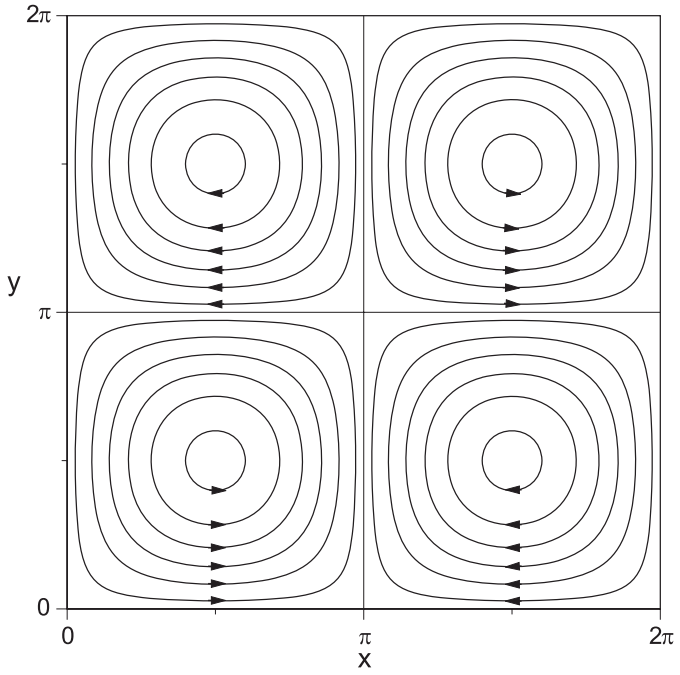

Figure 2. Streamlines of the flow field. Arrows indicate flow direction.

Equations (4) and (6) have been derived under general considerations and can be used to study the dumbbell motion in many two-dimensional flow conditions. In the present work the flow field is derived from the streamfunction ψ:

$$\psi(x, y) = U_o/k \sin kx \sin ky. \tag{12}$$

The corresponding velocity field at the point (x, y) is

$$\mathbf{u} = U_o(\sin kx \cos ky, -\cos kx \sin ky, 0) \tag{13}$$

with gravity aligned in the negative y direction. Figure 2 shows some typical streamlines. The flow consists of a periodic array of counter-rotating eddies which extend periodically in both x and y directions, with periodicity $2\pi/k$. The maximum velocity occurs at the cell boundaries and there are equilibrium points at the center of each cell and at the corners.

Taking U_o and $L = 1/k$ as characteristic velocity and length, respectively, the equations of motion for the dumbbell can be expressed in non-dimensional form. Non-dimensional variables and parameters are introduced as follows:

$$x_i^* = \frac{x_i}{L}, \qquad y_i^* = \frac{y_i}{L} \qquad d^* = \frac{d}{L}, \qquad R^* = \frac{R}{L} \tag{14}$$

$$t^* = t\frac{U_o}{L}, \qquad V^* = \frac{V}{U_o}, \qquad u_i^* = \frac{u_i}{U_0} \qquad W^* = \frac{W}{U_o}. \tag{15}$$

Now, equations (4) and (6), with the asterisks suppressed, take the form

$$\ddot{x} = A\left[\tfrac{1}{2}(\sin x_2 \cos y_2 + \sin x_1 \cos y_1) - V_x\right] \tag{16}$$

$$\ddot{y} = A\left[-\tfrac{1}{2}(\cos x_2 \sin y_2 + \cos x_1 \sin y_1) - V_y - W)\right] \tag{17}$$

$$\ddot{\theta} = A_r[-d\cos\theta(\cos x_2 \sin y_2 - \cos x_1 \sin y_1) - d\sin\theta(\sin x_2 \cos y_2 - \sin x_1 \cos y_1) - d^2\Omega], \tag{18}$$

where

$$x_1 = x - d/2\cos\theta, \qquad y_1 = y - d/2\sin\theta \tag{19}$$

$$x_2 = x + d/2\cos\theta, \qquad y_2 = y + d/2\sin\theta. \tag{20}$$

The angle θ specifies the orientation of the dumbbell in the (x, y) plane and A, A_r are non-dimensional parameters defined as

$$A = \frac{\beta L}{mU_o} \tag{21}$$

$$A_r = \frac{\beta L^3}{IU_o} = \frac{A}{\left(d^2 + \frac{2}{5}R^2\right)}. \tag{22}$$

Remembering that $d \gg R$, A_r can be expressed in a simplified form as

$$A_r = \frac{A}{d^2}, \tag{23}$$

and equation (18) takes the form

$$\ddot{\theta} = \frac{A}{d}[-\cos\theta(\cos x_2 \sin y_2 - \cos x_1 \sin y_1) - \sin\theta(\sin x_2 \cos y_2 - \sin x_1 \cos y_1)] - A\Omega. \tag{24}$$

Thus, for the translational motion of the dumbbell a Stokes number can be defined, $1/A$, which measures the dimensionless response time of the dumbbell to changes in the surrounding fluid while for the motion about the dumbbell mass center now appears a 'rotational' Stokes number, $1/A_r$, which has the same meaning as $1/A$ but referred to the angular velocity. Note that A_r cannot be regarded as an independent parameter as well as it depends on the dumbbell length, d. Thus, if the dumbbell length and A are both increased in such way that A_r decreases and the relation $A_r \ll A$ is fulfilled, the rotational dynamics becomes less sensitive to changes in the surrounding fluid. On the contrary if $d \ll 1$, irrespective of the value of A, it will be shown in the following sections that the dumbbell behaves as it were a single particle.

The three coupled nonlinear systems given by equations (16), (17) and (24) can be written as a nonlinear dynamical system as

$$\dot{\mathbf{X}} = \mathbf{f}(\mathbf{X}) \tag{25}$$

with $\mathbf{X} = (x, y, \theta, V_x, V_y, \Omega)$, $\mathbf{f} = (V_x, V_y, \Omega, f_1, f_2, f_3)$ and f_i $(i = 1, 2, 3)$ being the right-hand side of equations (16), (17) and (24) respectively. These equations were numerically integrated by using a fourth-order Runge–Kutta routine. The initial position and orientation of the dumbbell, (x_0, y_0, θ_0) were taken to be at random, while $\mathbf{V_0}$ and Ω_0 were such that the corresponding initial velocities of the beads $\mathbf{V_1}$ and $\mathbf{V_2}$ coincide with the fluid velocity at the bead positions.

3. Settling motion

Some examples of dumbbell trajectories for $A = 2$, $W = 0.5$ and three different values of the dumbbell length, d are shown in figures 3, 4 and 5.

Shown is a portion of the path after the dumbbell has reached the asymptotic state. The left side corresponds to the evolution of the dumbbell mass center and the right side represents the orientation angle versus the vertical coordinate y. The common feature of all these plots is

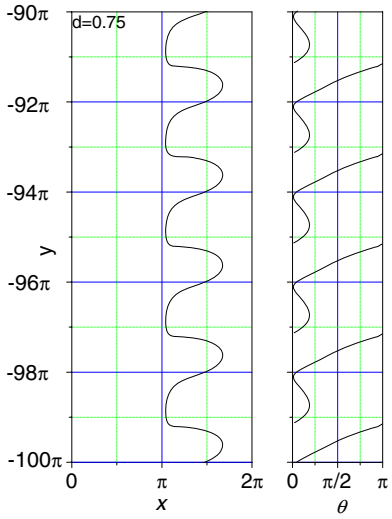

Figure 3. An example of dumbbell trajectory for the inertia parameter $A = 2$, single bead still fluid settling velocity $W = 0.5$ and bead-to-bead distance $d = 0.75$. Left side: path of the dumbbell mass center in the (x, y) plane. Right side: orientation angle θ versus the vertical coordinate y.

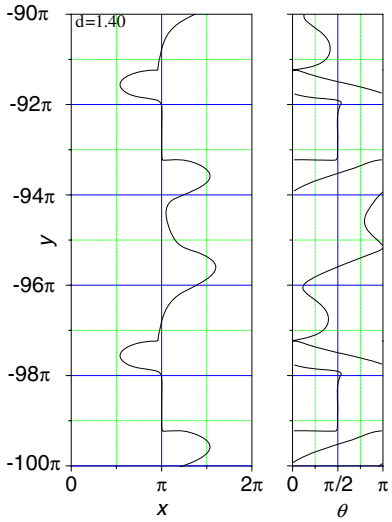

Figure 4. Similar as figure 3, for $A = 2$, $W = 0.5$ and $d = 1.40$.

that the motion is open. The dumbbell tends to contour the boundary of the eddies giving the trajectory a sinuous look. This feature emphasizes the importance of the flow field in driving the settling process. However, in all of the three examples the average motion is downward and thus gravity is still the dominating force.

Figure 3 corresponds to dumbbell length $d = 0.75$. In this case the dumbbell mass center follows a periodic trajectory. In general, it was observed that when the motion was periodic, the long-term regime is not sensitive to the choice of initial conditions. As was noted by

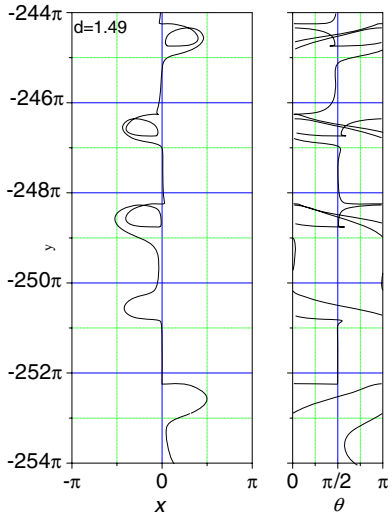

Figure 5. Similar as figure 3, for $A = 2$, $W = 0.5$ and $d = 1.49$.

Maxey [15] this phenomenon is due to the effects of inertia. Indeed, he observed that inertia induce a migration of particles toward the boundary of the cells were they collect on single isolated trajectories irrespective of their initial conditions.

The sinuosity of the dumbbell trajectory can be understood in terms of the location of the dumbbell beads in the cells. When the beads are in zones with upward flow they are submitted to a vertical drag force opposite gravity. In such circumstances, the net vertical force decreases or it may be directed upward. As a consequence the downward velocity slows down. During these intervals the settling process is interrupted and the dumbbell remains almost suspended. While this balance of the vertical force occurs, the dumbbell is driven horizontally by the net horizontal component of the drag force. On the other hand, when the beads are in downward zones of the flow, drag and gravity forces push the mass center downward and the effect of settling is increased. The general picture is that the force of gravity dominates most of the times and the dumbbell settles down.

The motion of the dumbbell in the vertical direction extends over a large range of cells. An alternative method of plotting that takes advantage of the periodic nature of the flow field consists of restricting the dumbbell motion to lie in the box $0 \leqslant x, y \leqslant 2\pi$. In this way, long portions of the path can be resumed in a single plot, allowing the immediate capture of essential features of the dumbbell dynamics, as for example, if the motion is periodic or not. The condensed path diagram thus obtained for the previous example is shown in figure 6. Here, the periodic nature of the motion becomes evident, with periodicity 2π in the vertical direction and horizontal amplitude lying in one cell length. Along this path the downward velocity of the dumbbell, plotted at the center of figure 6, varies over a large range with an average value larger than $W = 0.5$. This increased settling effect arises because the dumbbell spends most of the time in flow regions with downward velocities, also evident in the figure, where the drag force and gravity point in the same direction.

To show the evolution of the orientation angle, θ, a sketch of the dumbbell was drawn at several positions on the path. The condensed plot of θ at the right side of figure 6 confirms the periodical behavior. In this example, while the mass center runs over its path during a cycle, the dumbbell axis performs a complete turn.

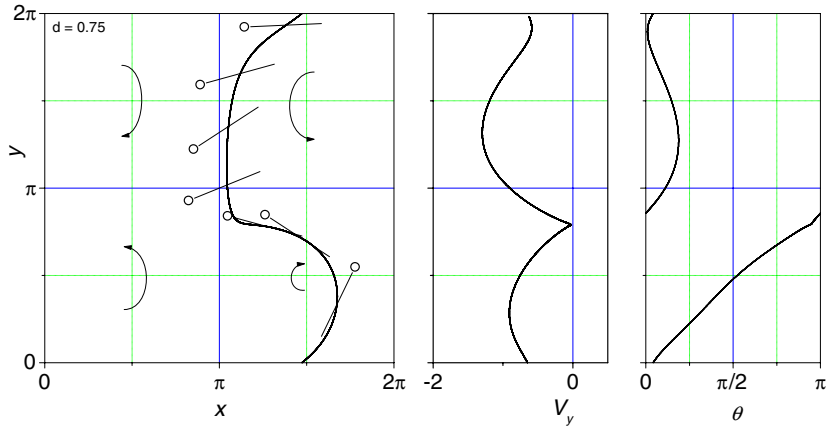

Figure 6. Condensed path diagrams for the dumbbell trajectory of figure 3. $A = 2$, $W = 0.5$ and $d = 0.75$. Left side: path of the dumbbell mass center in the reduced (x, y) plane. Right side: orientation angle θ versus the reduced vertical coordinate y. Arrows indicate the flow direction. The dumbbell was plotted at some successive position to illustrate the changing orientation.

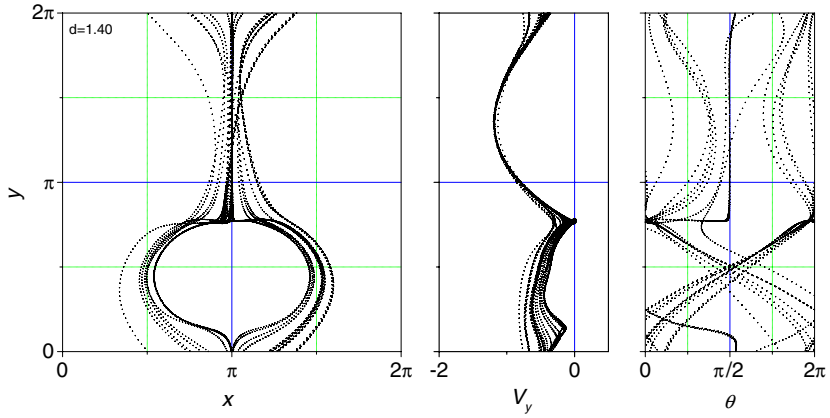

Figure 7. Condensed path diagrams for the dumbbell trajectory shown in figure 4. $A = 2$, $W = 0.5$ and $d = 1.40$.

The effect of increasing the dumbbell length can be seen in figure 4 for $A = 2$, $W = 0.5$ and $d = 1.4$. Here, the dumbbell mass center moves on a more intricate path. The motion is no longer periodic in the vertical direction. This effect can be clearly seen in the corresponding path diagram in figure 7. It is interesting to note that there are some paths where the dumbbell settles down vertically following the boundary line between cells, $x = \pi$. There, the orientation angle is $\theta = \pi/2$ which means that the dumbbell is oriented vertically. These vertical trajectories always begin at the intersection point of four cells and extend down to a point on the boundary line $x = \pi$ and below the horizontal line $y = \pi$. This ending point is particularly interesting because there, the vertical velocity goes to zero and the vertical dumbbell orientation rapidly switches from vertical to horizontal. Also note that the mass center is rapidly expelled to follow a more or less circular path. As a consequence of passing near the ending point, the dumbbell slows down and the average vertical velocity is lesser than in the previous case.

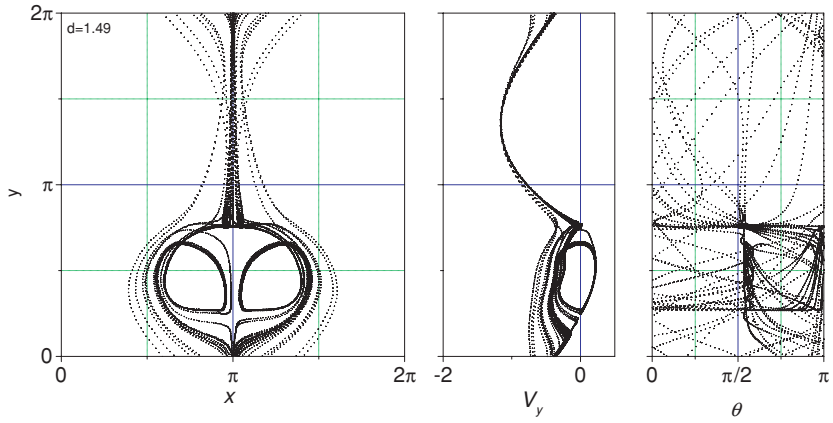

Figure 8. Condensed path diagrams for the dumbbell trajectory of figure 5. $A = 2$, $W = 0.5$ and $d = 1.49$.

Figures 5 and 8 show dumbbell dynamics for $A = 2$, $W = 0.5$ and $d = 1.49$. Note that now the path has lost any periodicity and the motion may be described as chaotic. The mass center of the dumbbell performs several loops where the settling motion is slowed down and, as in the previous case, it spends part of the time on the vertical boundary line where the angle orientation is $\theta = \pi/2$. When it approaches the ending point the vertical velocity goes to zero but in this case it is observed that there are periods of time (coincident with the occurrence of a loop) where the vertical velocity is directed upward. As a consequence, the settling motion slows down and the vertical average velocity takes the minimum value of the shown series.

The previous examples show that the settling motion is greatly affected by the dumbbell length d. This dependence as well as the influence of the other parameters will be studied in more detail in the following section.

4. Dependence of the settling motion with the dumbbell length

As shown in the previous section the vertical motion of the dumbbell results from the superposed effect of inertia, gravity and drag force. It was shown that for certain parameter combinations, the dumbbell mass center follows intricate paths and in consequence, the instantaneous mass center velocity, $V_y(t)$, results in very fluctuating functions of time. The relative influence of all the involved parameters is better captured if a global integral description of the settling motion is considered instead the instantaneous description given by $V_y(t)$. Thus, it is useful to introduce an average settling velocity, $\langle \mathrm{V}_y \rangle$, computed evaluating $V_y(t)$ for a large number of dumbbells distributed in random initial positions through the cells and then averaging over all of them once the asymptotic regime has been reached.

The value of $\langle \mathrm{V}_y \rangle$ thus obtained was computed for several sets of parameters A, d and W and the results are summarized in figures 9, 12 and 13.

For $A = 2$ and $W = 0.25$ the average velocity, $\langle \mathrm{V}_y \rangle$, for small values of d is approximately twice the still fluid settling velocity, W. In the limit when the bead-to-bead length tends to zero, the bead positions, $\mathbf{r_1}$, $\mathbf{r_2}$, approach $\mathbf{r}$ and then, equations (16) and (17) result

$$\ddot{x} = A[(\sin x \cos y - V_x] \tag{26}$$

$$\ddot{y} = A[-\cos x \sin y - V_y - W)]. \tag{27}$$

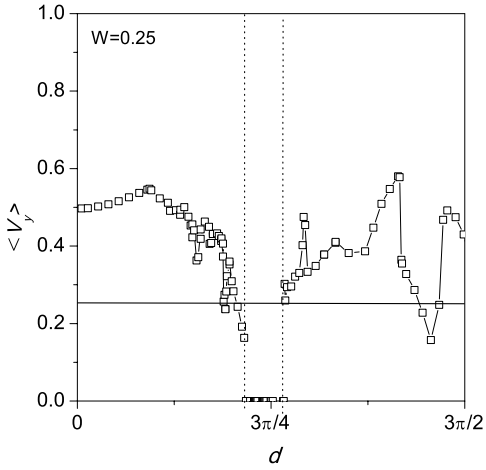

Figure 9. Average settling velocity $\langle V_y \rangle$ as a function of the dumbbell length, d for inertia parameter, $A = 2$ and still fluid settling velocity, $W = 0.25$.

Thus, for small d, the dynamics of the dumbbell mass center is equivalent to that of a single spherical particle and accordingly, the average velocity resulted similar to that computed by Maxey [15] for a single spherical particle in a cellular flow field under identical conditions of inertia and gravity. It should be noted that a decrease in d causes the approach of the spheres and thus some effects due to the interaction between them should appear. However, in the present formulation these effects were not included so the above result has to be understood as a necessary mathematical consequence of the model.

As d increases, the average settling velocity slightly increases and reaches its maximum value of $\langle V_y \rangle \simeq 0.55$ at $d \simeq 0.87$. A general feature of the motion in this range is that the orbits are periodic.

At $d = 0.87$ there is a transition from periodic to irregular trajectories. Figure 10 shows the power spectra, P, of the vertical velocity $V_y(t)$ for two values of the bead-to-bead distance after and before the transition. The power spectra describes how the power of a given signal is distributed over the frequency interval. It was computed from the usual definition:

$$P(f) = \frac{1}{\sum_{n=0}^{N-1} w(n)^2} B(f)^2, \tag{28}$$

where $B(f)$ is the FFT of the sampled data, $V_y(t)$ and $w(n)$ is the Hanning window: $w(n) = 1/2[1 - \cos(2\pi n/(N-1))]$. For $d = 0.8$ the power spectra reveal the periodic character of the motion. The main pick corresponds to $f = 1/T$ where T, the period of the path, is given by the ratio $T = \pi/\langle V_y \rangle$. On the contrary, the power spectra for $d = 0.9$ also present several distinguishable frequencies but they exhibit a noisy structure which is consistent with the irregular character of the motion. While a detailed study of irregular motions is beyond the scope of this work, it is worth noting that such complex dynamics could be expected because the system of equations (16), (17) and (24) represents a third-order autonomous dynamical system and this is the lowest order for an unforced dynamical system to exhibit chaotic motion [16].

For $d > 0.87$ the average velocity globally decreases and presents two local minima at $d = 1.45$ and $d = 1.8$. These events were not studied in detail but it was noted that they are

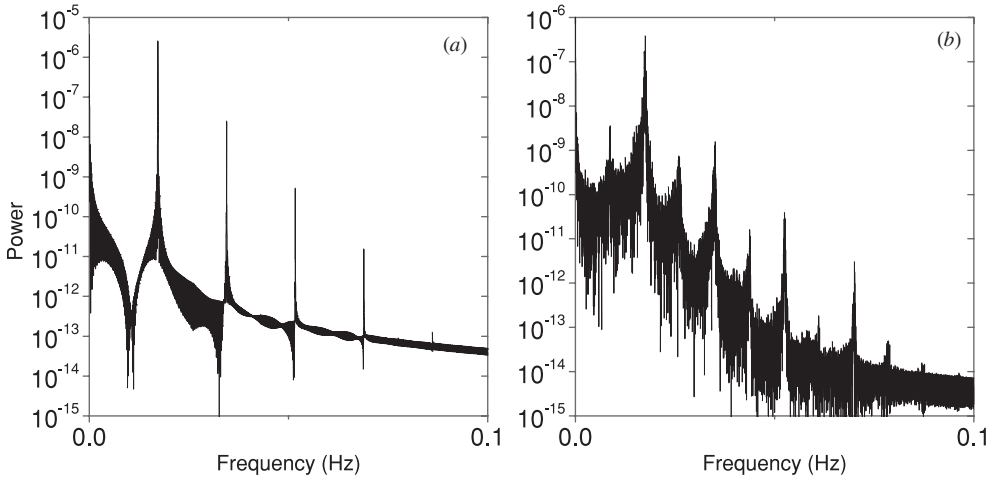

Figure 10. Power spectra of $V_y(t)$ for $A = 2$, $W = 0.25$ and for dumbbell lengths (a) $d = 0.8$; (b) $d = 0.9$.

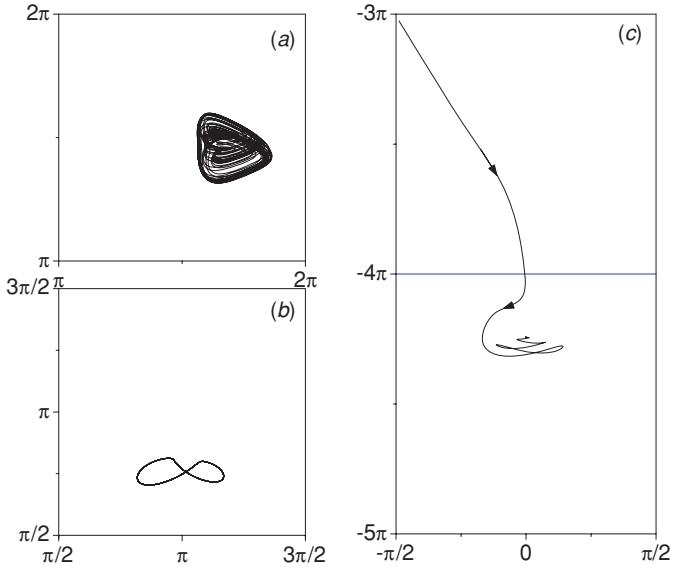

Figure 11. Center-of-mass trajectories in the suspension zone for $A = 2, W = 0.25$ and (a) $d = 2.16$, limited but open cycle, (b) $d = 2.17$, closed limit cycle, (c) $d = 2.19$, fixed point.

associated with local transitions between irregular and periodic behavior in the vicinity of the minima.

At approximately $d = 2.05$, $\langle V_y \rangle$ decays to zero and remains null up to $d = 2.51$. In this range, the dumbbells begin their motion settling out during a short time and then they enter into a trapping zone where they remain suspended indefinitely. The asymptotic paths may be classified into three types depending on the value of the dumbbell length, d: open but spatially limited orbits for $2.05 < d < 2.165$, limit cycles for $2.165 < d < 2.18$, or fixed points for $2.18 < d < 2.51$. Figure 11 shows examples of such behavior.

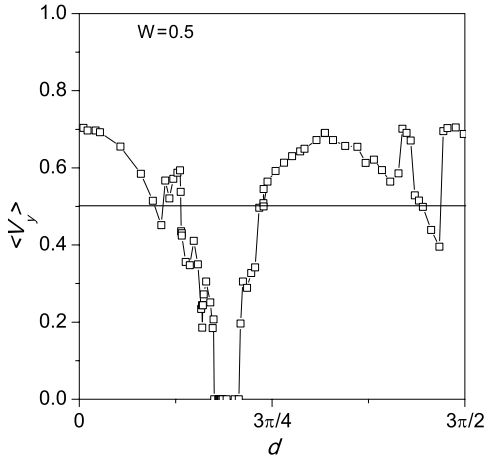

Figure 12. Average settling velocity $\langle V_y \rangle$ as a function of the dumbbell length, d for inertia parameter, $A = 0.2$ and still fluid settling velocity, $W = 0.5$.

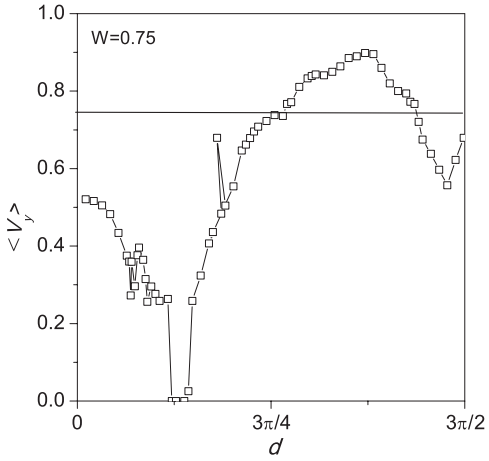

Figure 13. Average settling velocity $\langle V_y \rangle$ as a function of the dumbbell length, d for inertia parameter, $A = 0.2$ and still fluid settling velocity, $W = 0.75$.

For $d > 2.51$ the average velocity experiences a rapid transition to values generally larger than $W = 0.25$. In this range the curve is irregular and presents two sharp local maxima at $d = 2.75$ and $d = 3.92$. As in the previous case, these local maxima are associated with changes between irregular and periodic trajectories.

Figures 12 and 13 for $A = 2$, show the effect of increasing the value of the still fluid settling velocity, W. Results for $W = 0.5$ and $W = 0.75$ are presented. The graphs show similar transitions as in figure 9 for $W = 0.25$. The most important differences between the plots are the extension and location of the suspension region. As W is increased, the suspension range begins at smaller values of d and then extends over a narrow interval. In the limit $W = 1$ the suspension range converges to one single point in the limit $d = 0$. This point will be discussed later in section 5.

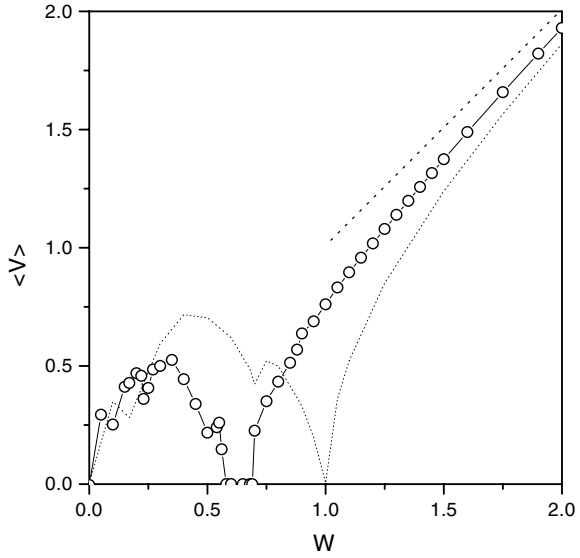

Figure 14. Average settling velocity $\langle V_y \rangle$ as a function of the still fluid settling velocity, W. Circles: $d = 1.3$; dotted-line: $d = 0$ (single-bead).

The influence of the still fluid settling velocity, W, for a fixed inertia parameter $A = 2$ and dumbbell length $d = 1.3$ can be seen in figure 14. For comparison, the settling velocity for a single spherical particle with $A = 2$, first studied by Maxey [15], was also plotted. This last case was obtained by setting $d = 0$ in equations (16) and (17), disregarding the effect of rotation. For this case it is observed that $\langle V_y \rangle$ initially increases and reaches a maximum somewhere about $W = 0.4$ before decreasing to higher values of W. As mentioned above, the settling velocity is zero at $W = 1$, then it increases again but always below the line $\langle V_y \rangle = W$ to approach this line asymptotically.

On the other hand, the settling velocity for the rigid dumbbell has a more intricate behavior. The graph of $\langle V_y \rangle$ goes through several local maxima and minima associated with changes in the periodicity of the trajectories in the range $0 < W < 0.58$. It presents a similar structure such as the plot of $\langle V_y \rangle$ for a single particle but with smaller values.

The interesting feature here is that the settling velocity is greater than W for $W < 0.61$. Under these circumstances the effect of gravity is small and the dumbbell is mainly driven for relatively large fluid forces. As a consequence, the dumbbell trajectory becomes twisted and it is capable of overcoming regions of upward flow. As it moves through zones of rapid downward flow the settling velocity is significantly increased.

As W increases, the influence of fluid forces decreases and the dumbbell is compelled to move in a more rectilinear path. Now the dumbbell is not capable of avoiding zones of upward flow and consequently the settling velocity is remarkably decreased.

About $W = 0.58$, the dumbbell passes through a stable equilibrium point and consequently the settling velocity drops to zero. This point marks the beginning of a wide suspension region which extends over the range $0.58 < W < 0.69$. Within this interval the dumbbell remains trapped into one of the three asymptotic paths described above.

For $W > 0.69$, the settling velocity increases monotonously but always below the value of the still fluid settling velocity W. As W becomes large, the influence of the fluid forces becomes negligible and the settling velocity asymptotically approaches the line $V_y = W$.

5. Equilibrium points and stability

Regarding the settling motion of the dumbbell in the cellular flow field, an important point to be considered is the existence of equilibrium or fixed points. A dumbbell which moves downward under the combined effects of gravity, drag and inertia will be slowed down or even it may be held stationary by the flow when it passes near a fixed point so that its settling properties such as the average settling velocity may be greatly affected. A fixed point occurs when the net force and torque vanish on the dumbbell. When applied in equations (16), (17) and (24) these conditions imply

$$0 = \sin(x_p + d/2\cos\theta_p)\cos(y_p + d/2\sin\theta_p) + \sin(x_p - d/2\cos\theta_p)\cos(y_p - d/2\sin\theta_p) \tag{29}$$

$$0 = \cos(x_p + d/2\cos\theta_p)\sin(y_p + d/2\sin\theta_p) + \cos(x_p - d/2\cos\theta_p)\sin(y_p - d/2\sin\theta_p)) + 2W \tag{30}$$

$$\begin{aligned} 0 = \cos\theta_p[&\cos(x_p + d/2\cos\theta_p)\sin(y_p + d/2\sin\theta_p) \\ &- \cos(x_p - d/2\cos\theta_p)\sin(y_p - d/2\sin\theta_p)] \\ &- \sin\theta_p[\sin(x_p + d/2\cos\theta_p)\cos(y_p + d/2\sin\theta_p) \\ &- \sin(x_p - d/2\cos\theta_p)\cos(y_p - d/2\sin\theta_p)], \end{aligned} \tag{31}$$

where, x_p, y_p and θ_p, are the coordinates of the fixed point. Although solutions of the above equations cannot be obtained for the general case, some particular cases with high symmetry can be analyzed with relative facility. As an example, consider the case $d = 0$ for which the dumbbell behaves as a single particle. The above equations reduce to

$$0 = \sin x_p \cos y_p \tag{32}$$

$$0 = \cos x_p \sin y_p + W. \tag{33}$$

Maxey [15] found that solutions of these systems are linearly unstable for all values of W except for $W = 0$ and $W = 1$ for which the fixed points are neutrally stable.

A simple example of fixed point with $d \neq 0$ can be obtained when the dumbbell is oriented perpendicular to the gravity ($\theta_p = 0$) with the mass center at some position (x_p, y_p). After some algebra the system reduces to

$$0 = \sin x_p \cos y_p \cos d/2 \tag{34}$$

$$0 = \cos x_p \sin y_p \cos d/2 + W \tag{35}$$

$$0 = \sin y_p \sin x_p \sin d/2. \tag{36}$$

Equilibrium points exist if $|\cos d/2| \leqslant W \leqslant 1$. Equation (34) and then equation (36) are immediately satisfied if $x_p = n\pi$ ($n = -1, 0, 1$). Substituting into equation (35) leads to

$$\sin y_p = (-1)^{n+1}\frac{W}{\cos d/2}. \tag{37}$$

The equilibrium points (x_p, y_p) together with the dumbbell bead positions are plotted in figure 15 as a function of the dumbbell length and for five different values of the terminal velocity W. In view of the periodicity of the system only the case $x_p = \pi$ is considered. Also note that the analysis is restricted to dumbbell lengths in the interval $0 \leqslant d \leqslant 2\pi$.

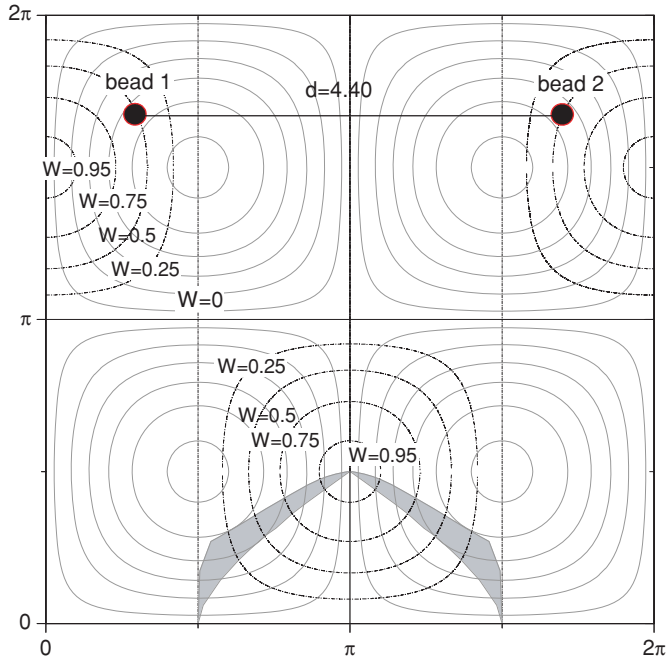

Figure 15. The position of the dumbbell beads for the horizontal fixed point $\theta = 0, x_p = \pi$ and, y_p given by equation (37) (with $n = 1$) for five different values of W. The sketched dumbbell corresponds to parameters $d = 4.4$ and $W = 0.5$. Gray filled areas correspond to stable fixed points.

To determine the stability of the equilibrium points, equation (25) was linearized around $\mathbf{X_p} = (\pi, y_p, 0, 0, 0, 0)$, where the value of y_p is obtained from equation (37). The resulting system can be written as

$$\dot{\mathbf{X}} = \mathbf{A}\mathbf{X}, \tag{38}$$

where $\mathbf{A}$ is the Jacobian matrix of f in equation (25) evaluated at $\mathbf{X_p}$. Solutions of the linearized system are proportional to $\exp(\lambda t)$ where the values of λ are the roots of the characteristic equation, $\det(\mathbf{A} - \lambda\mathbf{I}) = 0$. The fixed point is stable if and only if all the values of λ have negative real part. This condition implies that $\lambda_{\max}$, the maximum of the real part of eigenvalues, must be negative.

Figure 16 shows the plot of $\lambda_{\max}$ as a function of the dumbbell length, d for $A = 2$ and $W = 0.5$. For comparison the plot of $\langle V_y \rangle$ versus d was also superposed. It can be seen that there is a narrow region of d values where $\lambda_{\max}$ is negative corresponding to stable fixed points. In agreement, the average settling velocity, $\langle V_y \rangle$, is zero in this region. It is interesting to note the correlation existing between the curves. It is clear that while $\lambda_{\max}$ diminishes (increases), that is, as the fixed point becomes more stable (unstable) the value of $\langle V_y \rangle$ diminishes (increases), showing the stabilizing role played by the fixed point in the settling process.

Another interesting feature is that suspension occurs within an interval of d values which is larger than the stability interval corresponding to the horizontal fixed point. This result indicates that other mechanisms which lead the system to suspension must exist in addition to horizontal fixed point. As mentioned above, other possible modes of suspension are, open or

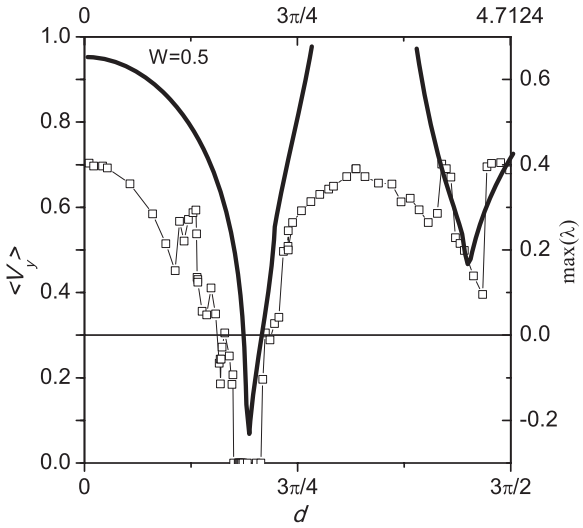

Figure 16. Value of the maximum of the real part of eigenvalues, $\lambda_{\max}$ as a function of d for $W = 0.5$ and $A = 2$. The results corresponding to $\langle V_y \rangle$ versus d were included for comparison.

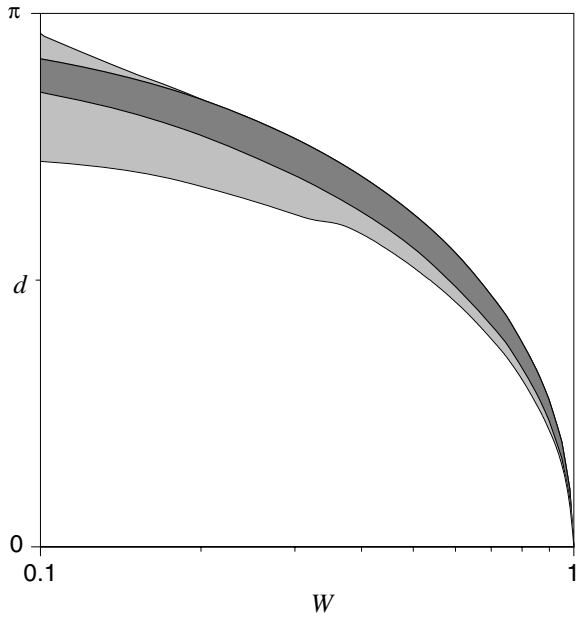

Figure 17. Stability diagram in the (W, d) plane for $A = 2$. The regions show the various modes for the dumbbell dynamics. Dark gray: suspension via the stable fixed point; light gray: suspension via open or closed limit cycles, white: settling motion with $\langle V_y \rangle > 0$.

closed limit cycles and non-horizontal fixed points. The diagram of figure 17 shows regions of stability on the parameter plane (W, d) for $A = 2$. Suspension occurs for parameters within the gray bands in the diagram. For parameters outside these bands the dumbbell settles out with $\langle V_y \rangle > 0$. The stable band can be subdivided into subregions according to the type of

mechanism that leads to suspension. Thus, the dark gray region corresponds to parameters for which the dumbbell is trapped by an horizontal fixed point. On the other hand, the light gray region corresponds to suspension via the other aforementioned mechanisms. This last region enlarges as W decreases indicating the importance of limit cycles (open or closed) in leading the system to suspension. On the contrary, as W increases, the thickness of the suspension band decreases until it becomes a single point for $W = 1$. This result emphasizes the increasing role played by this parameter in the settling process: the larger is the value of the still fluid settling velocity the smaller the possibility for dumbbells to come into the suspension mode.

6. Concluding remarks

In this work we have presented numerical results for a dumbbell-like particle settling under gravity in a cellular flow field. It was found that for given values of the inertia parameter, A, and the terminal velocity, W, the average settling velocity, $\langle V_y \rangle$, depend in a non-trivial way on the bead-to-bead distance d. For small d it was found that the trajectories are periodic but there is a transition to chaotic motion when d surpasses certain critical value. Additional increases in the length between spheres give place to successive transitions between periodic and chaotic trajectories. Another feature which is common of all the analyzed set of parameters is the occurrence of suspension for given ranges of the dumbbell length , d. It was shown that the regime of suspension is related to the existence of stable fixed point which in turn originates for the presence of a saddle point in the cellular flow. Even more, a correlation exists between the degrees of stability of this fixed point(given by $\lambda_{\max}$) and the value of the average settling velocity $\langle V_y \rangle$. However, it was observed that the fixed point is not the only mechanism which leads to suspension. Several other suspension states were found such as: open but limited orbit, closed limit cycles and also non-horizontal fixed points. These mechanisms were not studied in detail and their roles in the settling process will deserve special attention in future analysis.

The goal of this work was the construction of a simple physical model to evaluate the dynamics of non-spherical particles with the focus on the effects of inhomogeneous mass distribution. The assumption of $d \gg R$ allowed us to overcome the mathematical difficulties arising from considering the hydrodynamical interaction between the beads. However, this force should be taken into account in order to obtain a more complete description of the problem. According to reference [9], the interaction force between two identical beads writes

$$\mathbf{F_i} = -\beta(\mathbf{u}(\mathbf{r_i}) - \mathbf{v_i}) + \frac{3}{2}\frac{R}{d}\beta[(\mathbf{u}(\mathbf{r_i}) - \mathbf{v_i})\hat{\mathbf{n}}]\hat{\mathbf{n}}, \tag{39}$$

where $\hat{\mathbf{n}}$ is a unit vector perpendicular to the principal axis of the dumbbell. The proximity of the two beads modifies Stokes drag law by increasing the drag coefficient in the quantity $3/2R/d$ and by introducing a second term of order R/d which is non-parallel to the relative velocity. It is conjectured that this last term would affect the results presented here for $d \to 0$ as long as the restriction of vanishing R is eliminated. This point will deserve further analysis in the future work.

References

[1] Maxey M R and Riley J J 1983 Equation of Motion for small rigid sphere in a nonuniform flow *Phys. Fluids* **26** 883–9

[2] Cox R G 1965 The steady motion of a particle of arbitrary shape at small Reynolds number *J. Fluid Mech.* **14** 625–43

[3] Jianzhong L, Xing S and Zhenjiang Y 2003 Effects of the aspect ration on the sedimentation of a fiber in Newtonian fluids *J. Aerosol Sci.* **34** 909–21
[4] Hinch E J and Leal L G 1976 Constitutive equations in a suspension mechanics. Part 2. Approximate forms for a suspension of rigid particles affected by Brownian rotations *J. Fluid Mech.* **76** 187–208
[5] Jeffery G B 1922 The motion of ellipsoidal particles immersed in a viscous fluid *Proc. R. Soc. London Ser.* A **102** 161
[6] Lipscomb C G, Denn M M, Hur D U and Bogger D V 1988 *J. Non-Newt. Fluid Mech.* **26** 297–325
[7] Chiba K 2006 State of the art on flow kinematics and particle orientations during composite processing *J. Text. Eng.* **52** 227–36
[8] Mallier R and Maxey M R 1991 The settling of nonspherical particles in a cellular flow field *Phys. Fluids* A **3** 1481–94
[9] Happel J and Brenner H 1973 *Low Reynolds Number Hydrodynamics* (Leyden: Noordhoff) 242
[10] Bird R B, Curtiss C F and Armstrong R C 1987 *Dynamics of polymeric liquids* 2nd edn vol 2 (New York: Wiley)
[11] Piva M and Gabbanelli S 2003 A single dumbbell falling under gravity in a cellular flow field *J. Phys. A: Math. Gen.* **36** 4291–305
[12] Crisanti A, Falcioni M, Provenzale A, Tanga P and Vulpiani A 1992 Dynamics of passively advected impurities in simple two-dimensional flow models *Phys. fluids* A **4** 1805-
[13] Wang L P, Maxey M R, Burton T D and Stock D E 1992 Chaotic dynamics of particle dispersion in fluids *Phys. Fluids* A **4** 1789-
[14] Druzhinin O A and Ostrovsky L A 1994 The influence of Basset force on particle dynamics in two-dimensional flows *Physica* D **76** 34–43
[15] Maxey M R 1987 The motion of small spherical particles in a cellular flow field*Phys. Fluids* **30** 1915–28
[16] Guckenheimer J and Holmes P 1983 *Nonlinear Oscillations, Dynamical Systems and Bifurcations of Vector Fields* (New York: Springer)